

1 Introduction

This is a brief user’s manual for the source discretization scheme. Earthquake sources can be considered as combinations of smaller sources or *subevents*. As the observed seismic records at various stations may be reproduced by superimposing the wavetrains from the individual subevents, one may argue whether tsunami propagation from a large source can also be considered as a combination of tsunami waves from smaller subevents.

The **blocks** package is a set of codes and scripts that prepare the inputs and analyze the outputs of the MOST algorithm (Titov et al., 2016) for this application.

2 Method

Our method here is inspired by that used by NOAA (Gica et al., 2008; Titov et al., 2016). While we are using a similar idea, i.e., breaking down or *discretizing* the source into blocks, our discretization method is significantly different. In contrast with NOAA’s method, our approach is based on first calculating realistic Okada deformation and then breaking it down to components (as opposed to simply taking on several arbitrary sea floor blocks as tsunami sources).

While our approach seems to be valid only in retrospect (i.e., knowing the source structure), it serves our purpose in studying the effects of rupture resolution – especially allowing for comparison with real data.

In this approach, first the source surface deformation is calculated using an Okada method from a point source (strike, dip, slip, magnitude, depth). Then the calculated field will be broken into a mosaic of tiles of a given size (Fig. 1) for each of which the tsunami field will be calculated using the MOST algorithm.

At the end, calculated fields of maximum amplitude and time series

from all the tiles are superimposed to reproduce those from a single source. Finally the two sets of results are compared; these results should ideally be very similar as for instance shown in Fig. 2.

Finally the time series from both methods are calculated at common virtual gauges and compared using various metrics.

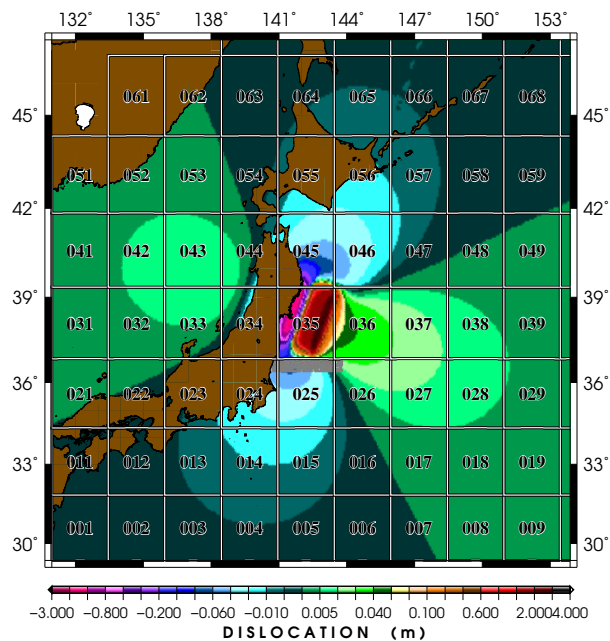


Figure 1: The Okada deformation for the 2011 Tohoku event (CMT) divided into a mosaic of 76 ($2.5^\circ \times 2.5^\circ$) tiles.

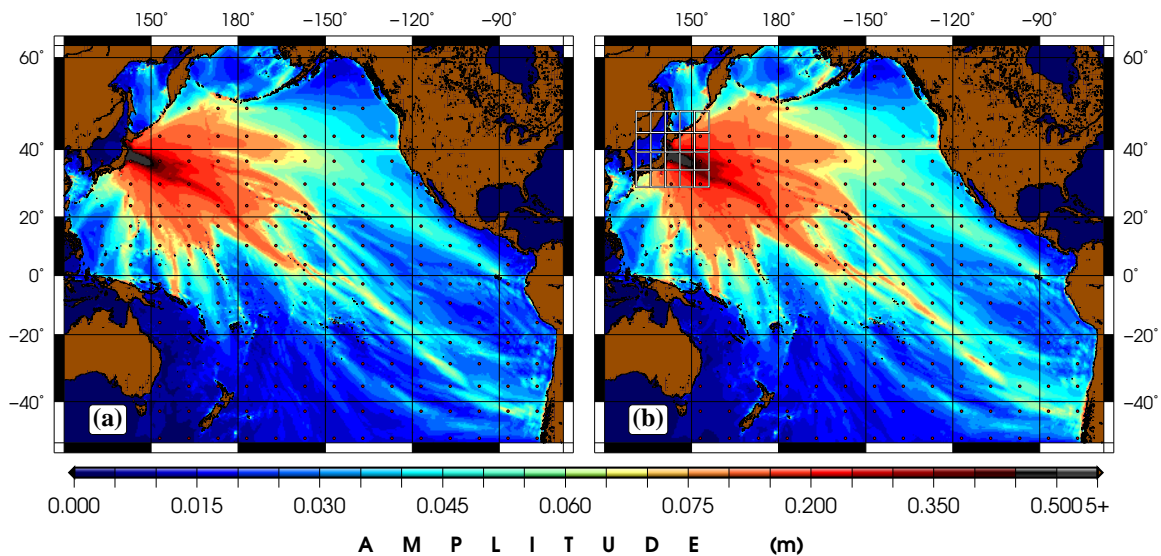


Figure 2: (a) Field of maximum tsunami amplitude from a full static source for the 2011 Tohoku earthquake; (b) the same field calculated and superimposed from individual fields of each tile. Red dots represent virtual gauges.

3 Software

This operation is best done on two machines.

To use the package, first you would need the main MOST input files (bathymetry and control) files in your working directory. Then you need a surface deformation file *for the entire basin* (which is also a MOST input). This file must be in the *burn.dat* format.

3.1 Making the Original Deformation Field

This is an exact same process for making the deformation file in MOST simulations. To achieve this, you would need the following:

- *BATH.dat*: Bathymetry file for the entire basin;
- *LON.LAT*: Bathymetry coordinates for the basin
- *smylie.out.z*: Local deformation file calculated for a point source.

The result, or *burn.dat* is the same local deformation interpolated within the bathymetry grid and will be an ASCII file with an $\mathbf{nx} \times \mathbf{ny}$ format (i.e. \mathbf{nx} altitude values in each line corresponding to a line of constant latitude).

Having a deformation field at hand, please follow through the following steps to use the package.

1. Use the **mesh.f** routine to divide the field into a mosaic of tiles. The code works by pinpointing the extent of deformation (the area where $z \neq 0$) and then breaking only that portion of the field into rectangular tiles. This is done to only focus the *tile work* at the source which is what we really want to discretize.

The user is asked for tile size along latitude and longitude.

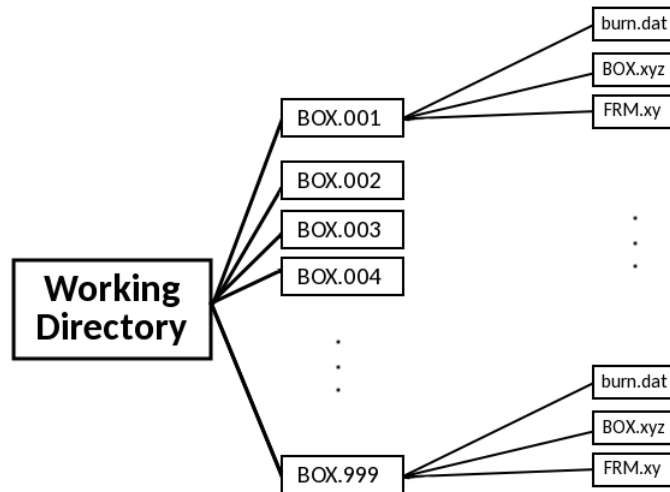
The code produces *four* groups of output:

- *burn.XXX.dat*: Isolated deformations inside each tile placed within the entire basin. This is used as the input deformation field by

MOST. *XXX* is the index number for the tile.

- *BOX.XXX*: Isolated deformation field only inside the individual tiles. These are XYZ files used for further analysis or plotting.
- *FRM.XXX*: The boundaris for each individual box indexed accordingly. These are in the form of four (lon,lat) pairs as the four corners of each box.
- *mesh.log* A log file containing information regarding a successful run.

2. Use the **movebox** script to organize the files into proper directories. This will move the files into the following structure:



3. In the working directory run the **generate** script which will create corresponding directories on `dizhi` and copy the files for run onto that machine.¹

¹This can be very time-consuming since you will be *uploading* the files. It is best to do this either from

Note: For this, the *copdizhi* alias will be used.

4. Now, on `dizhi` go to the working directory (see the structure shown above) under `MOST/block` and then run the `runbox` script. This will execute the MOST simulation. But remember that you will be limited by the number of processor cores on the machine (for instance `dizhi` has 16 cores which means you can only run 15 simulations at a time.²

To limit the number of simultaneous processes, type the maximum number while running the code:

```
./runbox [max._number]
```

If no number is specified, it will automatically be set to 15. For more details, see section 3.2 below.

5. To check up on the progress, use the `logger` script in the remote working directory. This will list the finished and running processes.
6. In order to retrieve the main simulation files (i.e. *max.out* and *gauges.out* from `dizhi`, in the working directory on the main machine run the `retrv` script. This will copy these files into their corresponding directories.
7. You can use the `maxadd.f` and `supgauge.f` programs to superimpose the retrieved outputs.

3.2 A Few Notes on the *runbox* Script

Here are a few notes when using the `runbox` script on the remote machine.

a fast network or from a machine on campus.

²It is best to reserve one of the cores for the operating system.

- There is a chance that the run would stop on the remote machine due to various reasons; so it is a good idea to keep an eye on the progress with the **logger** script. If you discover failed runs (i.e. if an ETA is frozen or everything seems to be unusually “done”), you can either run the few failed runs individually, or you can resume the run from the point it has failed.

To do this, simply type the index of the first failed run when running the script again:

```
./runbox [max._number] [first_failed_run]
```

Note that in this case, you also need to provide a value for the maximum number of simultaneous runs. This will resume the script from the first missing run.

- *Running Time Window*: I had initially foreseen that under *normal circumstances*(!) the full run for a mosaic source will not take more than 72 hours. If by any chance you find out that the script does not get to successfully finish all the runs due to this limit, simply tweak the number of time window by changing the *hr* variable in the script to your desired value.
- By default, the script will look for the number of simultaneous runs every 1 minute (60 seconds). This is set by the *slp* variable in the script – default is 60 seconds. To speed this up or slow it down, simply decrease or jack up this value to your liking.

3.3 The *mostsup* Script

Spatial superposition of tsunami simulation results is done using the **mostsup** script. *mostsup* adds up the fields of maximum amplitudes from the individual simulations in the order listed in the *list.box* file.

At each addition step, an *MT* value is calculated indicating a difference between the two grids before and after addition of the new block. Smaller *MT*

values indicate little changes and vice versa. Major contributions are selected as “large” jumps in the MT series. Here, I have set a default threshold of $MT = 0.3$ through trial and error from several trials. This is admittedly a bit subjective, but it is a first effort. The user can change this threshold by tweaking the *comp* variable at the beginning of the script.

Introduction of the MT metric into the software, provides us with a chance to identify and illustrate the major tsunami contributions from the sum of blocks. In this way the main contributors can easily be identified and illustrated. Here, such contributors are simply shown in red. As a next step, we can color-code the blocks according to their corresponding MT values.

To use this script simply copy it into a new directory (with an arbitrary name) in the working directory – where all the *BOX.XXXX* directories are located.

4 Case Study: 2011 Japan

Here is an example of TSD using the above approach for the 2011 Japan event. This event is chosen here since it was well-documented and well-studied. In the – near – future, we can compare our results for this event with the existing real data.

In this example, the deformation are is divided into 76 blocks to cover all the sea floor deformations from the event (see Fig. 1. Snapshots of the superposition process are shown in Fig. 3.

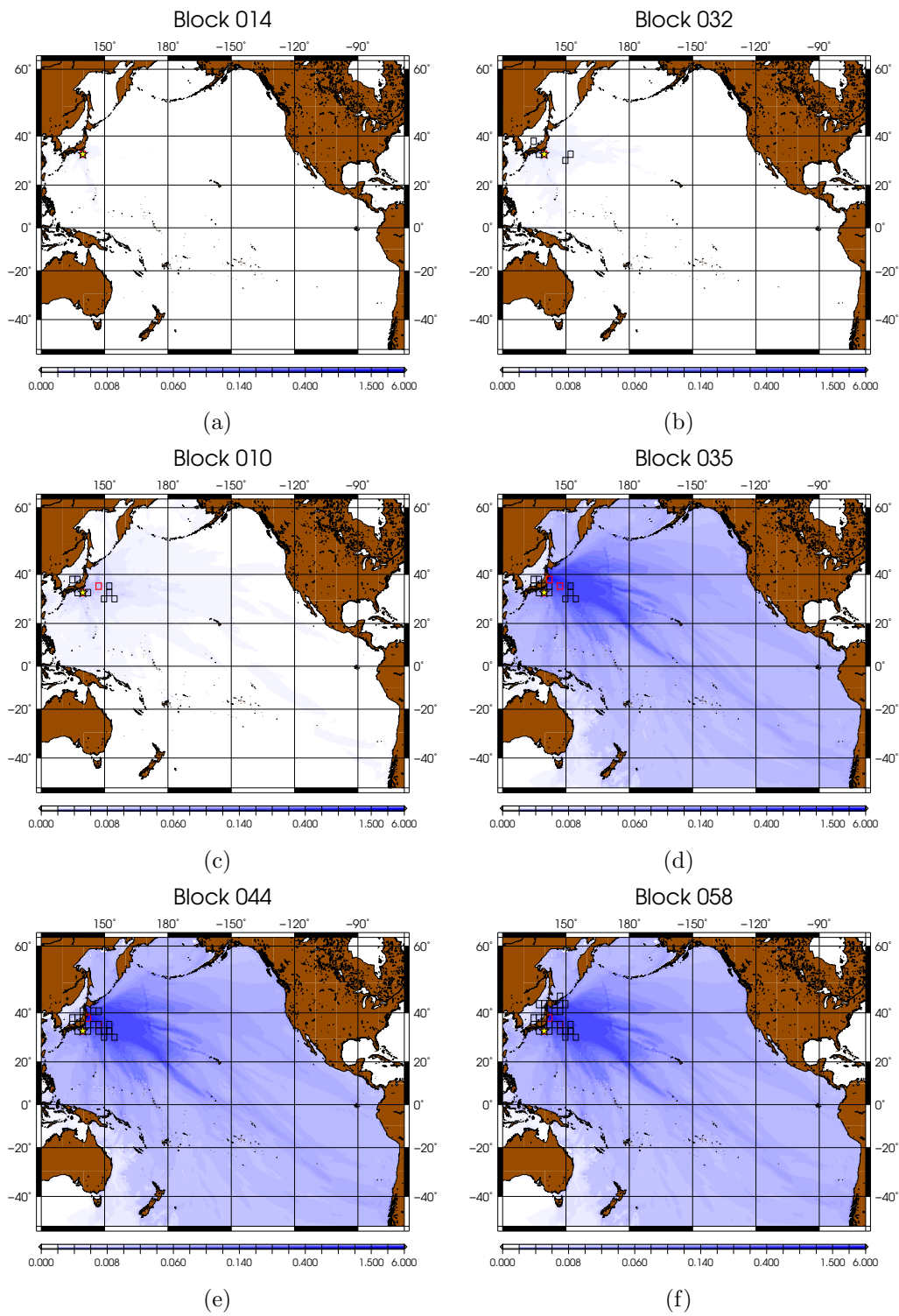


Figure 3: Snapshots of cumulative tsunami waveheights from a 31-part, fictional rupture in Japan. The block components are selected from Fig. 1.

A video of this fictional chaotic rupture is at <https://youtu.be/Hed2BG8S6LU>.

4.1 Time Lag

Temporal dependence of the tsunami is also examined. We note that in the absence of any time lags, the recorded time series at the virtual gauges (at least in the first pass) are identical between the fully static and block simulations. An example for a gauge near Japan is shown in Fig. 4.

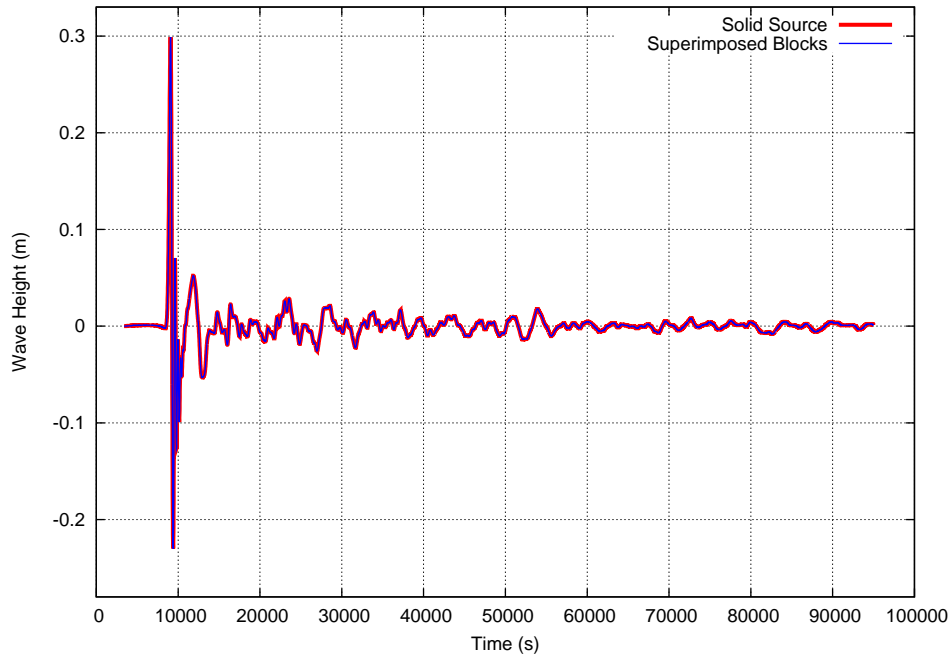


Figure 4: Comparison of the recorded time series at a gauge near Japan for fully static and block simulations.

However, even in the coarse geographic resolution of our mesh, time lags affect the time series. For instance, as shown in Fig. 5 the constituent blocks are given arbitrary time lags (without a physical meaning and simply as a test) compared to the origin time. We emphasize the completely arbitrariness

of these time lags as they are not based on any published or even physical model.

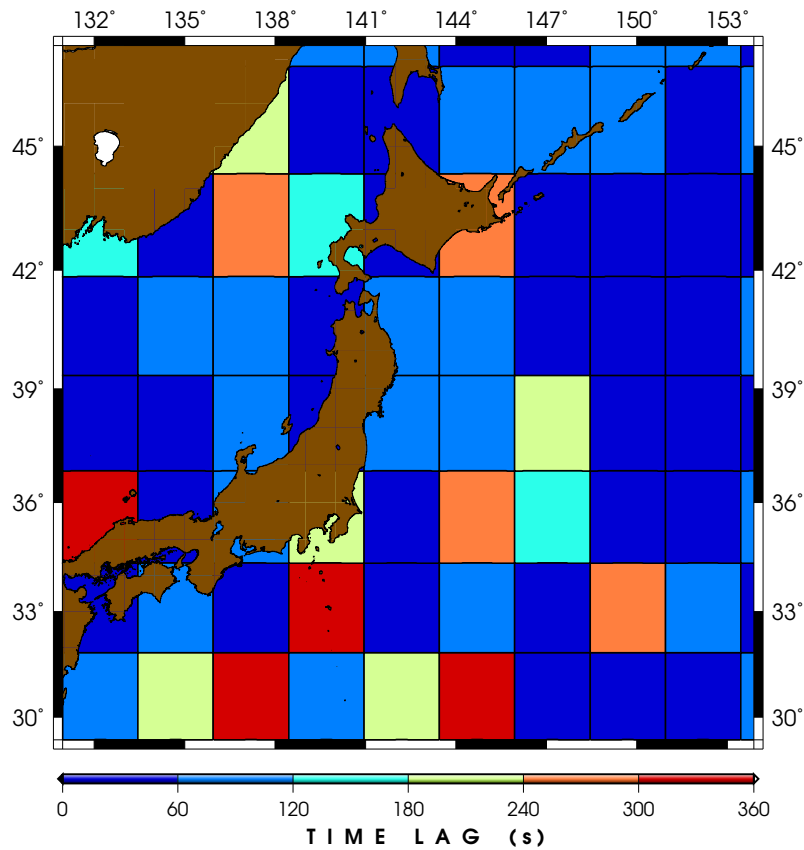


Figure 5: A fictional time lag distribution of the deformation mosaic shown in Fig. 1.

Then by applying the proposed time lags to the recorded time series from corresponding individual simulations a discrepancy is observed.

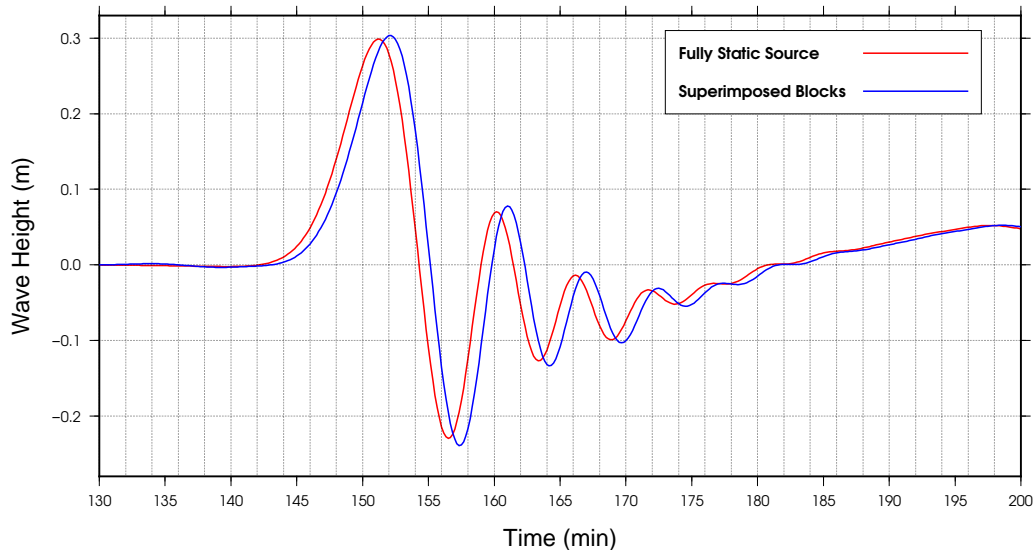


Figure 6: As a result of the fictitious time lags, the two series (for fully static and block simulations) have an ~ 1 minute difference.

While there seems to be a difference of approximately 1 minute between the two time series in Fig. 6,³ and there is about 5% mismatch in peak-to-peak amplitudes, I anticipate that these differences would increase in more realistic scenarios where the time lags are more systematic and localized (but of course, this is subject to further research).

4.1.1 Near-Field vs. Far-Field

In order to analyze the TSD effect with time lags on the near-field vs. far-field, one should look at both the wave amplitude and the period. In an effort to find a simple way to combine these effects I have introduced the parameter M_g . This was motivated by Richter’s (1935) effort to combine period and intensity variations in seismic shaking at various locations. Similar to the Prague formula, I define M_g as

³We note that in tsunami warning, 1 minute is a very long time.

$$M_g = -\log_{10}\left(\frac{A}{T}\right) + Q(\Delta, h_{sg}, s) \quad (1)$$

where A and T are the maximum amplitude (in meters) and dominant period of the corresponding tsunami wave arrival (in seconds) calculated at an open ocean gauge (similar to DART). $Q(\Delta, h_{sg}, s)$ is a constant determined by source-station distance (Δ), source and gauge bathymetries (h_{sg}), and source size (s). This is done to provide a constant value for M_g . Since for this analysis, we are not concerned with a universal *magnitude* for the tsunami, but are rather looking for the difference of wave trains at the same location for the time being I am setting $Q = 0$.

Using Eq. (1), one can readily calculate the metric for various gauges and map the M_g values in the basin for each scenario, i.e. fully static and kinematic ruptures. The results of such analyses are shown in Figs. 8a and 8b.

An immediate result from Fig. 8 (especiall Fig. 8c) is that the difference in the near-field is not significant, as expected. However, this could be due to the very coarse nature of our meshing scheme as our major source geometries are still isolated within whole tiles. *We shall investigate this as soon as the finer simulations are finished.*

An interesting feature of Fig. 8 however, is that the marked differences are not observed in very far-field, but are within what we may call an “*intermediate-field*”. This may have been caused by a variety of factors such as (1) directivity [as most of these *anomalies* are in directive azimuths], and (2) bathymetry [as the focusing effect of the mid-latitude trench and attoll systems in the Pacific may cause significant variations].

We can look more closely at (1) above by tweaking the meshing as well as source location. (2) can be resolved by working with a flat Pacific bathymetry.

4.1.1.1 Tsunami Magnitude

Finding an appropriate measure as *tsunami magnitude* is indeed an open debate as no valid and universal measure for tsunami magnitude has yet been proposed. This is mainly due to the fact that tsunami wave amplitude is more complex than that of the seismic waves due to the nature of the diffusion (rather than the wave-) equation. Also, since very few off-shore measurement stations for tsunami waves exist (Fig. 7) there is much less data available to study this concept in more detail.

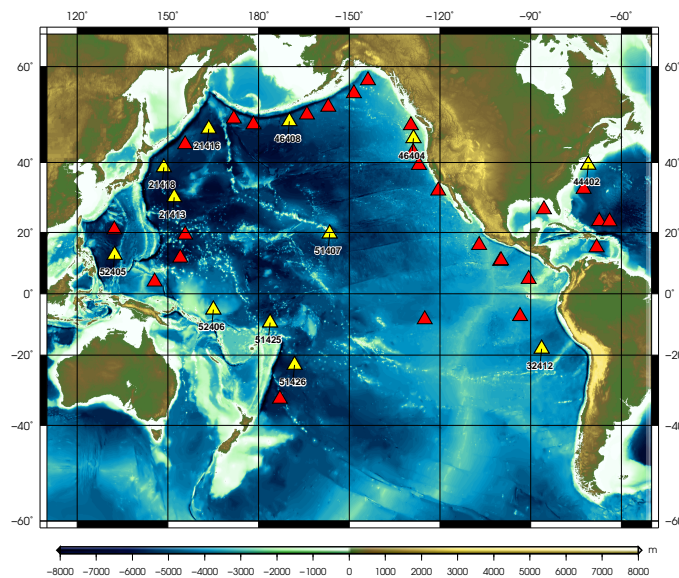


Figure 7: Installed DART buoys in the Pacific and the Caribbean. Statistically, only about $\sim 30\%$ of these instruments are operational. Yellow triangles denote the operational stations as of December 2018.

It should also be noted that similar to earthquakes, intensity scales have been proposed for tsunamis (e.g., Shuto, 1993; Papadopoulos & Imamura, 2001), but these are – just like earthquake intensity – subject to perception and lack a physical understanding of the source.

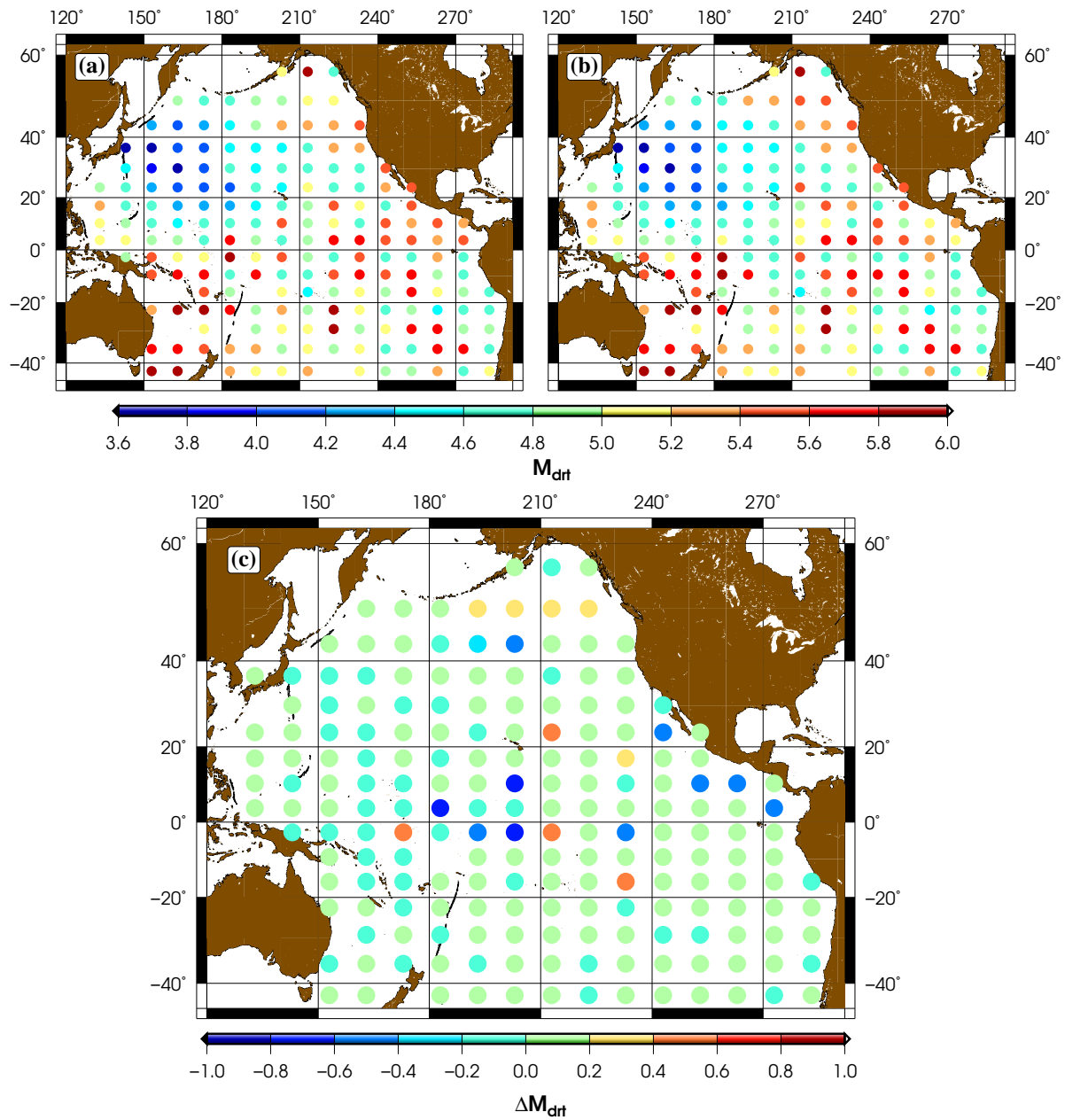


Figure 8: Calculated M_g values for (a) kinematic (Fig. 1) and (b) static sources. (c) the pointwise difference between (a) and (b).

5 The Next Step(?)

I think as the next step, we may

- Consider azimuthal dependence of observed tsunami time lags;
- Work at a higher resolution. Currently I am running a scenario with 387 building blocks. Next, I will be running another (already prepared) scenario with 1480 blocks (Fig. 9);

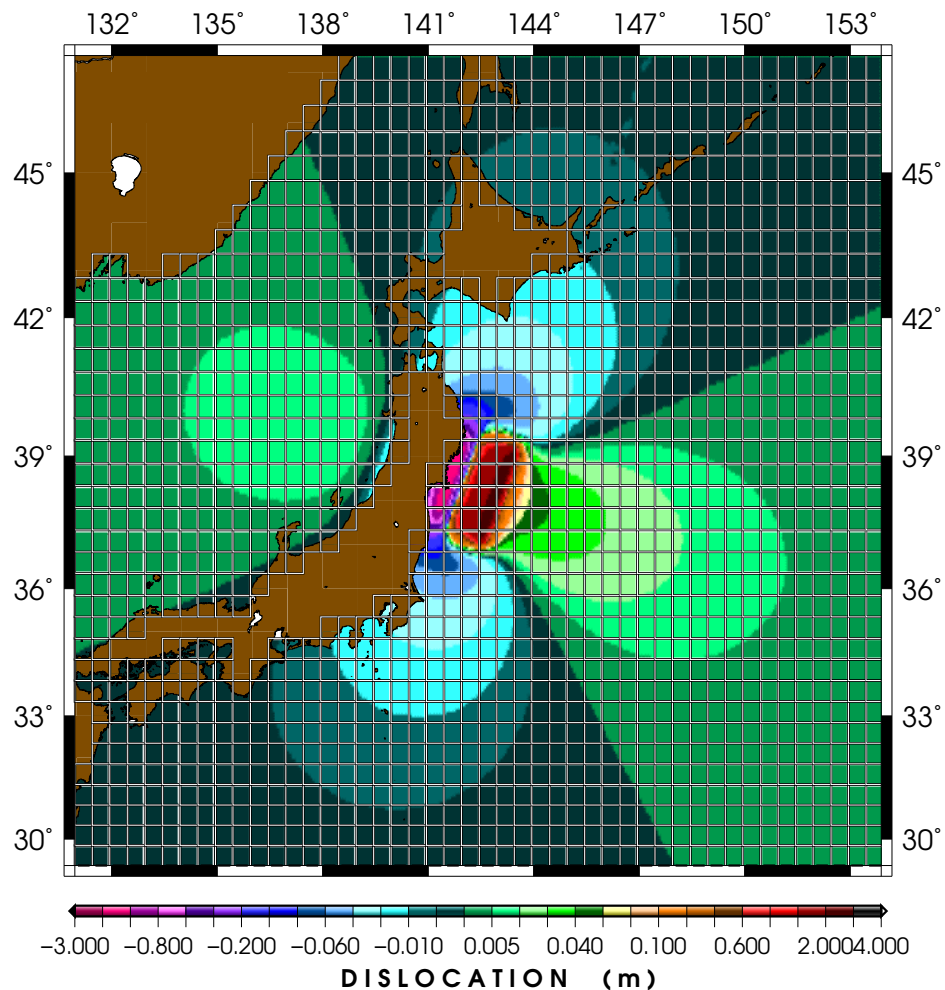


Figure 9: [similar to Fig. 1] The Okada deformation for the 2011 Tohoku event (CMT) divided into a mosaic of 1480 ($0.5^\circ \times 0.5^\circ$) tiles.

- Start looking at more realistic rupture scenarios. We can do this by working on slip inversion results. The challenge will be to calculate ocean floor deformations from such complex sources;
- Then, compare our results with real data;
- Finally work on other regions, e.g., Cascadia and Sumatra.
- Focus on the rupture area. So far, we have simulated tsunami wave

heights for Okada deformations in the entire source area. After finishing our full scale analyses, we can mesh only the rupture area.

- I think at this point it is a good idea to speed things up a bit. Since the current rate at which I am running simulations is only ~ 100 simulations per day, I propose running simulations on other machines (such as `wozhi`) as well. Maybe putting together a schedule for people running simulations on both machines is a good idea.(?)
- **Following the access to Williamson et al. (2019):** This article is a good first step (comparing to Melgar et al., 2019). But leaves several areas open to more work.

I think there is an excellent opportunity to:

1. Work in more detail on the intermediate-field idea;
2. Study the resolution in detail. Even Williamson et al. (2019) give a hand-waving statement as the more detail the merrier.
3. Do some beam-forming. I think a beam-forming approach can provide more insight into directivity.
4. Dig into our crude choice of six subevents – which is roughly what they have done – for Cascadia.

References

- Gica, E., Spillane, M. C., Titov, Vasily V., C. C. D., & Newman, J. C., 2008. Development of the forecast propagation database for NOAA's Short-term Inundation Forecast for Tsunamis (SIFT), *NOAA Technical Memorandum OAR PMEL-139*.
- Melgar, D., Williamson, A. L., & Salazar-Monroy, E. F., 2019. Differences between heterogenous and homogenous slip in regional tsunami hazards modelling, *Geophysical Journal International*, **219**(1), 553–562.
- Papadopoulos, G. A. & Imamura, F., 2001. A proposal for a new tsunami intensity scale, in *ITS 2001 proceedings*, vol. 5, pp. 569–577.
- Richter, C. F., 1935. An instrumental earthquake magnitude scale, *Bulletin of the Seismological Society of America*, **25**(1), 1–32.
- Shuto, N., 1993. Tsunami intensity and disasters, in *Tsunamis in the World*, pp. 197–216, Springer.
- Titov, V., Kânoğlu, U., & Synolakis, C., 2016. Development of MOST for real-time tsunami forecasting, *Journal of Waterway, Port, Coast and Oceanic Engineering*, **142**, 03116004–1–03116004–16.
- Williamson, A., Melgar, D., & Rim, D., 2019. The effects of earthquake kinematics on tsunami propagation, *JGR: Solid Earth*, [in review].